Chemical Communications

d0cc01136c

We have presented the graphical abstract image and text for your article below. This briefly summarises your work, and will be presented with your article online.

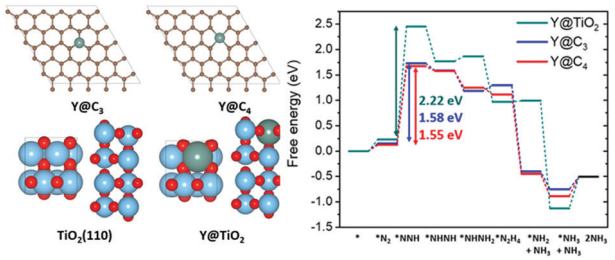

Single yttrium sites on carbon-coated TiO_2 for efficient electrocatalytic N_2 reduction

Lianghao Yang, Changhyeok Choi, Song Hong, Zhiming Liu, Zhenqing Zhao, Mengmeng Yang, Huidong Shen, Alex W. Robertson, Hao Zhang, Tsz Woon Benedict Lo, Yousung Jung* and Zhenyu Sun*

We report a facile synthesis of single yttrium sites anchored on carbon-coated TiO_2 for efficient and stable electrocatalytic N_2 fixation.

Q2

Please check this proof carefully. Our staff will not read it in detail after you have returned it.

Please send your corrections either as a copy of the proof PDF with electronic notes attached or as a list of corrections. **Do not edit the text within the PDF or send a revised manuscript** as we will not be able to apply your corrections. Corrections at this stage should be minor and not involve extensive changes.

Proof corrections must be returned as a single set of corrections, approved by all co-authors. No further corrections can be made after you have submitted your proof corrections as we will publish your article online as soon as possible after they are received.

Please ensure that:

- The spelling and format of all author names and affiliations are checked carefully. You can check how we have identified the authors' first and last names in the researcher information table on the next page. **Names will be indexed and cited as shown on the proof, so these must be correct.**
- Any funding bodies have been acknowledged appropriately and included both in the paper and in the funder information table on the next page.
- All of the editor's queries are answered.
- Any necessary attachments, such as updated images or ESI files, are provided.

Translation errors can occur during conversion to typesetting systems so you need to read the whole proof. In particular please check tables, equations, numerical data, figures and graphics, and references carefully.

Please return your **final** corrections, where possible within **48 hours** of receipt following the instructions in the proof notification email. If you require more time, please notify us by email to chemcomm@rsc.org.

Funding information

Providing accurate funding information will enable us to help you comply with your funders' reporting mandates. Clear acknowledgement of funder support is an important consideration in funding evaluation and can increase your chances of securing funding in the future.

We work closely with Crossref to make your research discoverable through the Funding Data search tool (http://search.crossref.org/funding). Funding Data provides a reliable way to track the impact of the work that funders support. Accurate funder information will also help us (i) identify articles that are mandated to be deposited in **PubMed Central (PMC)** and deposit these on your behalf, and (ii) identify articles funded as part of the **CHORUS** initiative and display the Accepted Manuscript on our web site after an embargo period of 12 months.

Further information can be found on our webpage (http://rsc.li/funding-info).

What we do with funding information

We have combined the information you gave us on submission with the information in your acknowledgements. This will help ensure the funding information is as complete as possible and matches funders listed in the Crossref Funder Registry.

If a funding organisation you included in your acknowledgements or on submission of your article is not currently listed in the registry it will not appear in the table on this page. We can only deposit data if funders are already listed in the Crossref Funder Registry, but we will pass all funding information on to Crossref so that additional funders can be included in future.

Please check your funding information

The table below contains the information we will share with Crossref so that your article can be found *via* the Funding Data search tool. **Please check that the funder names and grant numbers in the table are correct and indicate if any changes are necessary to the Acknowledgements text.**

Funder name	Funder's main country of origin	Funder ID (for RSC use only)	Award/grant number
National Natural Science Foundation of China	China	501100001809	21972010
University of Oxford	United Kingdom	501100000769	EP/R010145/1

Q1

Researcher information

Please check that the researcher information in the table below is correct, including the spelling and formatting of all author names, and that the authors' first, middle and last names have been correctly identified. **Names will be indexed and cited as shown on the proof, so these must be correct.**

If any authors have ORCID or ResearcherID details that are not listed below, please provide these with your proof corrections. Please ensure that the ORCID and ResearcherID details listed below have been assigned to the correct author. Authors should have their own unique ORCID iD and should not use another researcher's, as errors will delay publication.

Please also update your account on our online manuscript submission system to add your ORCID details, which will then be automatically included in all future submissions. See here for step-by-step instructions and more information on author identifiers.

First (given) and middle name(s)	Last (family) name(s)	ResearcherID	ORCID iD
Lianghao	Yang		
Changhyeok	Choi		0000-0002-7181-3100
Song	Hong		0000-0002-8532-3348
Zhiming	Liu		
Zhenqing	Zhao		
Mengmeng	Yang		
Huidong	Shen		
Alex W.	Robertson	J-5321-2014	0000-0002-9521-6482
Hao	Zhang		
Tsz Woon Benedict	Lo		
Yousung	Jung	D-1676-2010	0000-0003-2615-8394

Zhenyu	Sun		0000-0001-5788-9339

Queries for the attention of the authors

Journal: **ChemComm**

Paper: **d0cc01136c**

Title: **Single yttrium sites on carbon-coated TiO_2 for efficient electrocatalytic N_2 reduction**

For your information: You can cite this article before you receive notification of the page numbers by using the following format: (authors), Chem. Commun., (year), DOI: 10.1039/d0cc01136c.

Editor's queries are marked on your proof like this Q1, Q2, etc. and for your convenience line numbers are indicated like this 5, 10, 15, ...

Please ensure that all queries are answered when returning your proof corrections so that publication of your article is not delayed.

Query reference	Query	Remarks
Q1	Funder details have been incorporated in the funder table using information provided in the article text. Please check that the funder information in the table is correct.	
Q2	Please confirm that the spelling and format of all author names is correct. Names will be indexed and cited as shown on the proof, so these must be correct. No late corrections can be made.	
Q3	*Chem. Commun.* communications have a strict 4 page limit. If your article exceeds this limit, please trim the article to fit. Some content could be changed to electronic supplementary information (ESI) if necessary.	

ChemComm

COMMUNICATION

Single yttrium sites on carbon-coated TiO_2 for efficient electrocatalytic N_2 reduction†

Cite this: DOI: 10.1039/d0cc01136c

Received 12th February 2020,
Accepted 5th August 2020

DOI: 10.1039/d0cc01136c

rsc.li/chemcomm

Lianghao Yang,[a] Changhyeok Choi,[b] Song Hong,[c] Zhiming Liu,[a] Zhenqing Zhao,[a] Mengmeng Yang,[a] Huidong Shen,[a] Alex W. Robertson,[d] Hao Zhang,[e] Tsz Woon Benedict Lo,[e] Yousung Jung *[b] and Zhenyu Sun *[a]

We report single yttrium sites anchored on carbon-coated TiO_2 for efficient and stable electrocatalytic N_2 fixation, delivering an NH_3 faradaic efficiency exceeding 11.0% and an NH_3 yield rate as high as 6.3 μg_{NH_3} h^{-1} $mg_{cat.}^{-1}$ at low overpotentials, thus surpassing many reported metal electrocatalysts.

Ammonia (NH_3) is one of the most important industrial chemicals used in agricultural, pharmaceutical, and synthetic fiber sectors.[1] It is also a carbon-neutral liquid fuel with high energy density and is readily liquefiable.[2] However, the industrial production of ammonia is still dependent on the Haber–Bosch (HB) process *via* the reaction of N_2 and H_2 at a high temperature (300–500 °C) and pressure (200–350 atm), leading to massive fossil fuel consumption, excessive CO_2 emission, and intense capital inputs. Electrochemical N_2 reduction to NH_3 using renewably generated electricity under mild conditions is a promising alternative approach to the conventional Haber–Bosch process, and it has sparked increasing research interest in recent years.[3–18]

To activate the strong and nonpolarizable N≡N bond, rational design and development of high-performance catalysts is key. An effective electrocatalyst should exhibit a stronger binding ability towards nitrogen than towards hydrogen to inhibit the parasitic hydrogen evolution reaction (HER),[6] and drive the injection of more electrons into the N_2 antibonding orbitals to accelerate the nitrogen reduction reaction (NRR). Despite recent efforts in this regard, most catalytic systems that have been reported to date suffer from large overpotential for NH_3 formation, low N_2 adsorption and reduction activity. Atomically dispersed atom catalysts have recently attracted intensive attention owing to the maximum metal utilization efficiency, homogeneity of catalytically active sites, tunable coordination environment and electronic structure of metal atoms.[19,20] These distinct advantages endow single-atom catalysts with superior catalytic performance for many energy conversion reactions. Nonetheless, only a limited number of single-atom electrocatalysts have been explored for NH_3 synthesis.[6,21]

Herein we report a facile synthesis of isolated Y atoms immobilized on porous carbon-coated TiO_2. The supported single Y sites can greatly facilitate the NRR to NH_3 in an acidic electrolyte at room temperature and atmospheric pressure. This catalyst delivered a large NH_3 faradaic efficiency (FE) of 11.2 ± 0.5% and an NH_3 yield rate of about 6.3 ± 0.2 μg_{NH_3} h^{-1} $mg_{cat.}^{-1}$ at a low applied potential (−0.22 V *vs.* the reversible hydrogen electrode, RHE), outperforming many reported transition metal-based electrocatalysts. All the potentials shown in this work are relative to the RHE scale unless stated otherwise.

Isolated yttrium (Y) atoms on porous carbon-wrapped TiO_2 (denoted as Y-TiO_2-C) were fabricated through a simple hydrothermal method followed by annealing under Ar (ESI†). Fig. S1 shows the X-ray diffraction (XRD) patterns of the as-prepared Y-TiO_2-C and pure TiO_2. Only the diffraction peaks of the tetragonal rutile phase (JCPDS 21-1276) were observed for pristine TiO_2, while some amounts of the anatase phase were identified in the Y-TiO_2-C samples, indicating that the introduction of Y and C inhibited the transformation of anatase to rutile at high temperatures. No typical peaks of metallic Y and Y_2O_3 were found, ruling out the formation of Y-based aggregates and agglomerates. X-ray photoelectron spectroscopy (XPS) was conducted to probe the surface chemical state of the samples. As shown in the upper panel of Fig. S2a (ESI†), two pronounced peaks at 464.7 and 459.0 eV are observed, attributed to the Ti $2p_{1/2}$ and Ti $2p_{3/2}$ orbitals of TiO_2.[22] Compared to pristine TiO_2,

[a] State Key Laboratory of Organic–Inorganic Composites, Beijing University of Chemical Technology, Beijing 100029, P. R. China. E-mail: sunzy@mail.buct.edu.cn
[b] Department of Chemical and Biomolecular Engineering, Korea Advanced Institute of Science and Technology (KAIST), Daejeon 34141, Republic of Korea
[c] Analysis Technology R&D Center, Beijing University of Chemical Technology, Beijing 100029, P. R. China
[d] Department of Materials, University of Oxford, Oxford OX1 3PH, UK
[e] Department of Applied Biology and Chemical Technology, The Hong Kong Polytechnic University, Hong Kong, P. R. China

† Electronic supplementary information (ESI) available. See DOI: 10.1039/d0cc01136c

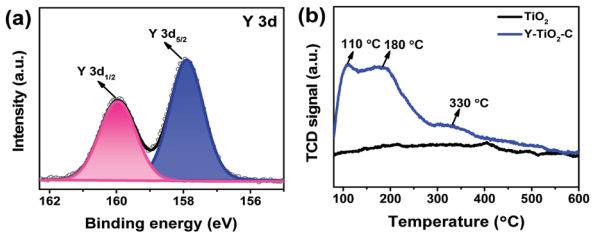

Fig. 1 (a) Y 3d XPS spectrum of Y-TiO_2-C. (b) N_2-TPD profiles of TiO_2 and Y-TiO_2-C. The loading of Y in the Y-TiO_2-C samples is 1.7 wt%.

the peaks of Ti 2p for Y-TiO_2-C show a positive shift of 0.4 eV, indicating the occurrence of electron transfer from TiO_2 to Y. Fig. S2b (ESI†) presents the C 1s XPS spectrum, in which the peaks at 284.9, 286.5, and 289.3 eV can be assigned to the C–C, C–O, and C═O moieties, respectively.[23] Deconvolution of the O 1s XPS spectra for both TiO_2 and Y-TiO_2-C revealed three peaks appearing at about 530.2, 531.5, and 532.9 eV, which originate from the Ti–O bond, surface chemisorbed oxygen, and OH– groups, respectively (Fig. S2c, ESI†).[11] Note that Y-TiO_2-C showed a lower percentage of chemisorbed oxygen species relative to pure TiO_2, indicating its fewer oxygen defects. Fig. 1a displays the Y 3d XPS spectrum, which consists of a doublet of Y $3d_{5/2}$ (157.9 eV) and Y $3d_{1/2}$ (159.9 eV), corresponding to Y^{3+}.[24]

Furthermore, Raman spectroscopy measurements showed three peaks in the range of 200–700 cm^{-1} for both TiO_2 and Y-TiO_2-C, including two Raman active modes (A_{1g} and E_g) and one multiphonon mode (M) (Fig. S3a, ESI†). The M peak shifted from 233 to 258 cm^{-1} while the E_g peak shifted from 448 to 412 cm^{-1}, which is likely associated with the strong charge interaction between TiO_2 and Y. Two peaks at 1302 and 1584 cm^{-1} are shown for Y-TiO_2-C and TiO_2-C, attributed to the disorder carbon (D band) and graphitic carbon (G band), respectively (Fig. S3b, ESI†). The pore structure of Y-TiO_2-C was analyzed by N_2 adsorption/desorption (Fig. S4, ESI†). A typical type II isotherm in the BDDT classification was observed for Y-TiO_2-C. The adsorption in the relative pressure (P/P_0) range $\leq$ 0.01 was attributed to microporosity, whereas the sharp adsorption–desorption hysteresis loop at $P/P_0 > 0.8$ was related to the mesopores *via* a capillary condensation mechanism. The BET surface area was estimated to be 355.2 $m^2\ g^{-1}$ and the average BJH (Barrett–Joyner–Halenda) pore diameter (the inset of Fig. S4, ESI†) was calculated to be about 5.5 nm from the desorption branch of the isotherm. The N_2 temperature programmed desorption (TPD) measurements (Fig. 1b) showed that Y-TiO_2-C exhibits a substantially higher N_2 adsorption capacity than TiO_2. The desorption peaks at 110 and 180 °C can be ascribed to N_2 physisorption, whilst the peak at 330 °C corresponds to N_2 chemisorption. In sharp contrast, only very weak N_2 adsorption signals were detected on TiO_2. Evidently, N_2 chemical adsorption and activation could be greatly facilitated by the as-obtained single Y site system, benefiting the NRR.

Transmission electron microscopy (TEM) (Fig. 2a) and high-resolution TEM images, along with fast Fourier transform (FFT)

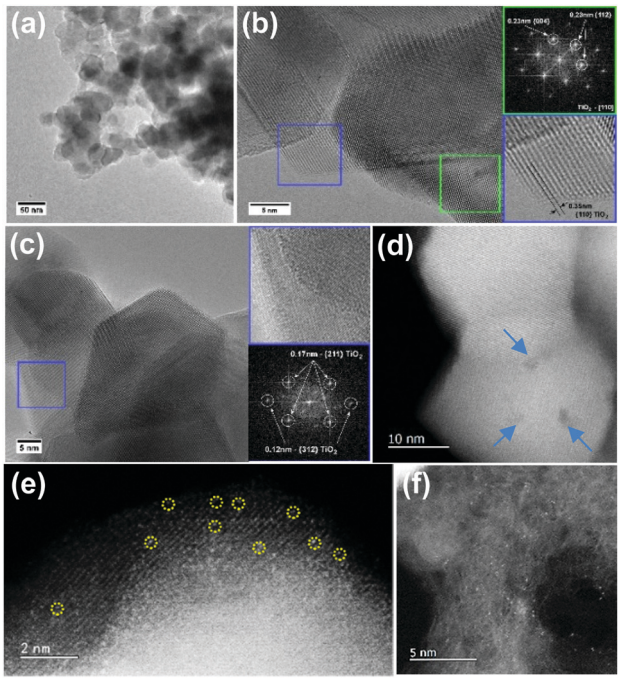

Fig. 2 (a) Low-magnification TEM image of Y-TiO_2-C. (b and c) HRTEM images with the corresponding magnified images and FFTs of the square areas of Y-TiO_2-C. (d) Low-magnification HAADF-STEM image of Y-TiO_2-C with pores highlighted in blue arrows. HAADF-STEM images of single Y atoms anchored on (e) the surface of TiO_2 and (f) the porous carbon layer on TiO_2.

images (Fig. 2b and c), confirmed the formation of the anatase phase TiO_2 nanoparticles with good crystallinity. Furthermore, high-angle annular dark-field scanning TEM (HAADF-STEM) observations together with energy-dispersive X-ray spectroscopy (EDS) elemental maps (Fig. S5, ESI†) revealed the presence of many bright spots distributed on the surface of TiO_2 (circled in yellow as shown in Fig. 2e) and also encapsulated into the porous carbon layer on TiO_2 (Fig. 2f). These spots can be assigned to the single Y atoms given the larger atomic number of Y than those of both Ti and C, and thus brighter appearance as revealed by STEM.

The Y-TiO_2-C catalysts were examined for NRR using a classic H-type cell separated by a Nafion 117 membrane. No N_2H_4 was detected by the Watt and Chrisp method and only NH_4^+ ions were identified by the indophenol blue method (Fig. S6 and S7, ESI†). From the linear sweep voltammetry (LSV) results (Fig. 3a), Y-TiO_2-C was observed to display a significantly higher current than TiO_2-C, Y-TiO_2, and TiO_2 in 0.1 M N_2-saturated HCl, indicating its superior NRR capability. The NRR began with an overpotential of $\leq$180 mV (Fig. 3b). The NH_3 formation rate over the catalysts increased from −0.12 to −0.22 V, but it decreased upon further improving the overpotential due to the more severe competing HER (Fig. 3b). Note that the maximum NH_3 formation rate over Y-TiO_2-C reached 6.3 ± 0.2 $\mu g_{NH_3}\ h^{-1}\ mg_{cat.}^{-1}$ at −0.22 V, in contrast to that of 2.38 $\mu g_{NH_3}\ h^{-1}\ mg_{cat.}^{-1}$ for pure TiO_2, which also remarkably outperformed TiO_2-C and Y-TiO_2 (Fig. 3b). The NH_3 FE was 11.2 ±

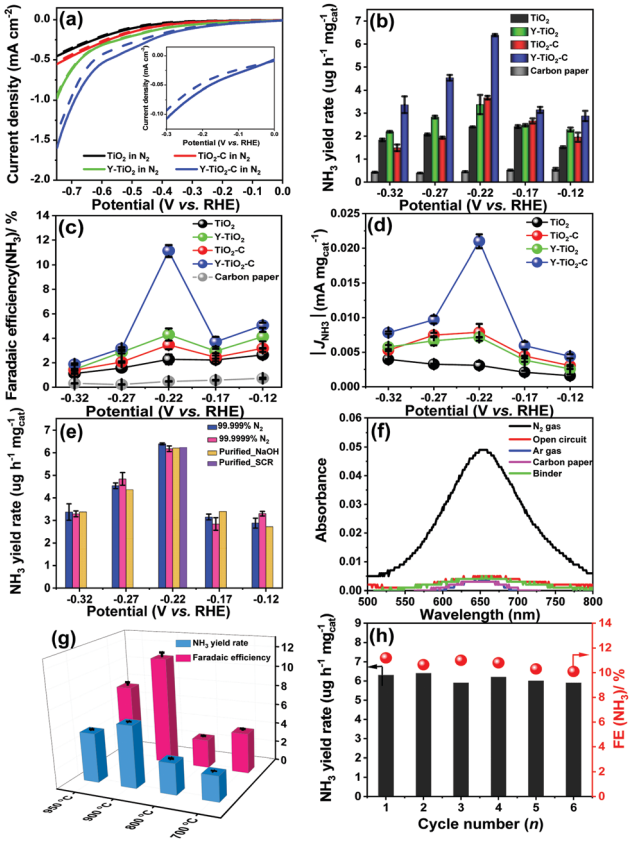

Fig. 3 (a) LSV curves of Y-TiO_2-C, Y-TiO_2, TiO_2-C, and TiO_2 in Ar-(dashed line) or N_2-(solid line) saturated 0.1 M HCl solution at a scan rate of 5 mV s^{-1}. (b) Yield rates and (c) FEs of NH_3 over Y-TiO_2-C, Y-TiO_2, TiO_2-C, TiO_2, and carbon paper. (d) NH_3 partial current densities over Y-TiO_2-C, Y-TiO_2, TiO_2-C, TiO_2, and carbon paper at various potentials. (e) Comparisons of the NH_3 yield rates at different applied potentials over Y-TiO_2-C using a feed gas of 99.999% N_2, 99.9999% N_2, and purified 99.9999% N_2 with 10 M NaOH or by SCR. (f) UV-Vis absorption spectra of the electrolyte after electrolysis at −0.22 V in either Ar-saturated electrolyte (Ar gas), or without the catalyst (carbon paper), or with the binder (binder), or at an open circuit potential (open circuit). (g) Effects of the annealing temperature on the NRR in terms of the NH_3 FE and the formation rate at −0.22 V over Y-TiO_2-C. (h) Cycling stability at −0.22 V over Y-TiO_2-C.

0.5% at −0.22 V, over 5.6 times as high as that of pristine TiO_2 (Fig. 3c). Likewise, the NH_3 partial current density was 20.0 μA cm^{-2}, 6.6 times higher than that of TiO_2 (Fig. 3d). The generation of NH_3 was also confirmed by NMR spectroscopy (Fig. S8, ESI†). The NH_3 yield rate was determined to be about 6.6 μg_{NH_3} h^{-1} mg_{cat}^{-1} by ^1H NMR, consistent with the value obtained by the indophenol blue method. Notably, Y-TiO_2-C outperforms most of the previously reported TiO_2-based materials[25–32] and many other transition metal and precious metal electrocatalysts in terms of the NH_3 FE (Fig. S9a and Table S1, ESI†).

To probe possible interferences, if any, from the environment and confirm the origin of the formed NH_3, multiple blank and control experiments were carried out. N_2 with a greater purity (99.9999%, Fig. S6b, ESI†) was used as a feed gas. Similar NH_3 yield rates and FEs were observed (Fig. 3e and Fig. S9b, ESI†). The N_2 (99.9999%) was further purified by selective catalytic reduction (SCR) of NO_x with NH_3[33] followed by removal of the remaining NH_3 or adsorption with 10 M NaOH solution to remove any possible NO_x in the feed gas. Almost equivalent NH_3 formation rates and FEs were observed (Fig. 3e and Fig. S9b, ESI†). These indicate that the trace impurities in the feed gas did not have an impact on the yield of NH_3 here. Almost no NH_3 was detected either in Ar-saturated solution, in the absence of catalyst, with just the background Nafion solution binder, or at an open circuit potential (Fig. 3f). The influence of possible contamination from the air was also ruled out by the observation that marginal NH_4^+ was detected after exposure of the electrolytes in the air for extended periods (Fig. S9c, ESI†). We further conducted isotopic labeling measurements using $^{15}N_2$ (99.0% $^{15}N{\equiv}^{15}N$) as the feed gas. The ^1H NMR spectrum of the NRR product displays a doublet coupling (~73 Hz) for $^{15}NH_4^+$ as opposed to a triplet coupling (~52 Hz) for $^{14}NH_4^+$ (Fig. S10, ESI†).[1] These results strongly suggest that the NH_3 was generated from the reduction of dissolved N_2 accelerated by the single Y sites.

The impact of Y content was studied for the NRR, the results of which showed that the optimal Y loading was 1.7 wt% (Fig. S11a and b, ESI†). The most favourable annealing temperature for the NRR was found to be 900 °C (Fig. 3g). We also found that both the NH_3 yield rate and FE increased steadily with the increase of the NRR temperature from 3 ± 3 to 60 ± 3 °C (Fig. S11c, ESI†). This indicates that faster kinetics dominated the reaction process at higher temperatures, thus boosting the NRR. The NH_3 yield rate and the FE reached 7.2 μg_{NH_3} h^{-1} $mg_{cat.}^{-1}$ and 12.0%, respectively, at 60 ± 3 °C.

To test the stability of Y-TiO_2-C, we conducted alternating electrolysis between Ar and N_2-saturated electrolytes. The evolved NH_3 could remain unchanged for 6 cycles (Fig. S11d, ESI†). The catalyst also maintained good stability with a nearly constant NH_3 production rate and FE even after 6 cycles in N_2-saturated 0.1 M HCl (Fig. 3h). XRD measurements showed that the crystalline structure of Y-TiO_2-C was largely maintained regardless of electrolysis (Fig. S1a, ESI†). Furthermore, chronoamperometry measurements revealed negligible decay in the total current after continuous electrolysis for 30 h (Fig. S12, ESI†). To gain insight into the outstanding activity of Y-TiO_2-C, the Tafel plot and electrochemical impedance were evaluated. The Tafel slope was ~162.6 mV dec^{-1} for Y-TiO_2-C (Fig. S13a, ESI†), much lower than those of TiO_2 (~304.9 mV dec^{-1}) and TiO_2-C (262.7 mV dec^{-1}). This implies that the single Y site catalyst exhibits more rapid reaction kinetics, and that the first electron transfer process to yield $*N_2H$ (* signifies the surface adsorbed species) is the rate-determining step.[16] Nyquist plots (Fig. S13b, ESI†) revealed a significantly lower charge transfer resistance for Y-TiO_2-C than for TiO_2-C, Y-TiO_2, and TiO_2, in accordance with its observed superior NRR activity. We also investigated the NRR over Y-TiO_2-C under neutral (0.1 M Na_2SO_4) (Fig. S14a, ESI†) and alkaline conditions (0.1 M KOH) (Fig. S14b, ESI†). Y-TiO_2-C was found to exhibit NRR activities in both cases, albeit with a lower NH_3 yield rate and FE compared to the values obtained in 0.1 M HCl

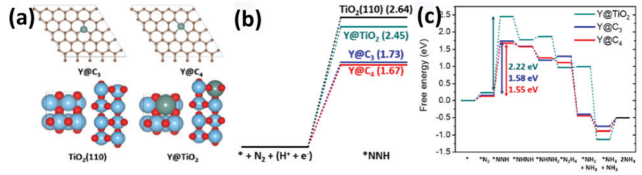

Fig. 4 (a) Optimized geometries of the adsorbed N_2 on Y@C_3, Y@C_4, TiO_2(110), and Y@TiO_2. The adsorption energy of N_2 at each site is listed in parenthesis (ΔE in eV). The green, sky blue, brown red, and blue balls represent the Y, Ti, C, O, and N atoms, respectively. (b) Formation free energy of *NNH (G(*NNH) − G(*) − $G(N_2(g))$) at Y@C_3, Y@C_4, TiO_2(110), and Y@TiO_2 (eV). (c) Free energy diagram for the NRR. The black, green, blue, and red lines indicate TiO_2(110), Y@TiO_2, Y@C_3, and Y@C_4, respectively.

solution, probably due to the lower concentration of protons available for the NRR.

We further performed density functional theory (DFT) calculations to investigate the origin of the improved NRR activity at single Y sites. We modelled single Y atoms anchored at a single-vacancy of carbon (Y@C_3) and a double-vacancy of carbon (Y@C_4) in graphene to construct atomic Y sites embedded in a carbon layer, while the Y doped rutile TiO_2(110) surface (Y@TiO_2) was considered for constructing atomic Y sites in TiO_2 (Fig. 4a). We first focused on the N_2 adsorption ability at the single Y sites (Fig. S15, ESI†). N_2 was chemically adsorbed at all single Y sites with an adsorption energy (ΔE) of −0.23 (Y@C_3), −0.25 (Y@C_4), and −0.15 eV (Y@TiO_2), respectively. However, N_2 was physically adsorbed on TiO_2(110) with a ΔE of −0.04 eV. This result is in agreement with the N_2-TPD profiles (Fig. 1b), which demonstrate increased N_2 chemisorption of Y-TiO_2-C than that of TiO_2. Next, we compared the formation free energy of *NNH denoted as ΔG(*NNH) (Fig. 4b) since the formation of *NNH is known as a potential-determining step (PDS) in various catalysts.[34–36] The ΔG(*NNH) increases in the order Y@C_4 (1.67 eV) < Y@C_3 (1.73 eV) < Y@TiO_2 (2.45 eV) < TiO_2(110) (2.64 eV). The *NNH is stabilized more favourably at Y@C_x sites than that of TiO_2(110) by ∼1 eV, indicating enhanced activation of N_2 at the Y@C_x sites. The full reaction free energy diagram of the NRR also shows a superior catalytic activity of the Y@C_x sites (Fig. 4c). The free energy change at the PDS (ΔG_{PDS}) increases following the sequence of Y@C_4 (1.55 eV) < Y@C_3 (1.58 eV) < Y@TiO_2 (2.22 eV), which illustrates markedly decreased ΔG_{PDS} at the Y@C_x sites compared to those of TiO_2(110) and Y@TiO_2. This is consistent with the experimental trend of Y-TiO_2-C > Y-TiO_2 > TiO_2 in terms of the NH_3 yield rate. Based on a combination of increased N_2 chemisorption, more stabilized *NNH, and decreased ΔG_{PDS} at the Y@C_x sites, the single Y atoms embedded in the carbon layers are believed to play an important role in boosting the NRR performance.

In summary, we have demonstrated a facile synthesis of atomically dispersed Y on porous carbon-coated TiO_2. Such a single site catalyst leads to strong N_2 adsorption and efficient NRR to NH_3 at low overpotentials under ambient conditions. A remarkably high FE over 11.0% with a reasonable NH_3 formation rate of 6.3 ± 0.2 μg_{NH_3} h^{-1} $mg_{cat.}^{-1}$ was achieved at −0.22 V (*vs.* RHE). This work provides a potential alternative avenue for sustainable N_2 fixation.

This work was supported by the National Natural Science Foundation of China (No. 21972010), the Beijing Natural Science Foundation (No. 2192039), and the DCCEM at the Materials Department, University of Oxford (EP/R010145/1).

Conflicts of interest

The authors declare no conflicts of interest.

Notes and references

1 S. Z. Andersen, V. Čolić, S. Yang, J. A. Schwalbe, A. C. Nielander, J. M. McEnaney, K. Enemark-Rasmussen, J. G. Baker, A. R. Singh, B. A. Rohr, M. J. Statt, S. J. Blair, S. Mezzavilla, J. Kibsgaard, P. C. K. Vesborg, M. Cargnello, S. F. Bent, T. F. Jaramillo, I. E. L. Stephens, J. K. Kørskov and I. Chorkendorff, *Nature*, 2019, **570**, 504.
2 J. Guo and P. Chen, *Chem*, 2017, **3**, 709–712.
3 K. Liu, H. Zhong, S. Li, Y. Duan, M. Shi, X. Zhang, J. Yan and Q. Jiang, *Prog. Mater. Sci.*, 2018, **92**, 64–111.
4 Y. Li, J. Zheng, Y. Lyu, M. Qiao, J. P. Veder, R. D. Marco, J. Bradley, R. Wang, A. Huang and S. Wang, *Angew. Chem., Int. Ed.*, 2019, **58**, 2–8.
5 Y. Yao, S. Zhu, H. Wang, H. Li and M. Shao, *J. Am. Chem. Soc.*, 2018, **140**, 1496–1501.
6 H. Tao, C. Choi, L. X. Ding, Z. Jiang, Z. Han, M. Jia, Q. Fan, Y. Gao, H. Wang, A. W. Robertson, S. Hong, Y. Jung, S. Liu and Z. Sun, *Chem*, 2019, **5**, 204–214.
7 J. Wang, L. Yu, L. Hu, G. Chen, H. Xin and X. Feng, *Nat. Commun.*, 2018, **9**, 1795.
8 Y. Lin, S. Zhang, Z. Xue, J. Zhang, H. Su, T. Zhao, G. Zhai, X. Li, M. Antonietti and J. Chen, *Nat. Commun.*, 2019, **10**, 1–7.
9 S. Chen, S. Perathoner, C. Ampelli, C. Mebrahtu, D. Su and G. Centi, *Angew. Chem., Int. Ed.*, 2017, **56**, 2699–2703.
10 C. Lv, C. Yan, G. Chen, Y. Ding, J. Sun, Y. Zhou and G. Yu, *Angew. Chem., Int. Ed.*, 2018, **57**, 6073–6076.
11 Z. Han, C. Choi, S. Hong, T. S. Wu, Y. L. Soo, Y. Jung, J. Qiu and Z. Sun, *Appl. Catal., B*, 2019, **257**, 117896.
12 Z. Sun, R. Huo, C. Choi, S. Hong, T. Wu, J. Qiu, C. Yan, Z. Han, Y. Liu, Y. Soo and Y. Jung, *Nano Energy*, 2019, **62**, 869–875.
13 M. Yang, R. Huo, H. Shen, Q. Xia, J. Qiu, A. Robertson, X. Li and Z. Sun, *ACS Sustainable Chem. Eng.*, 2020, **8**, 2957–2963.
14 Y. Liu, Y. Su, X. Quan, X. Fan, S. Chen, H. Yu, H. Zhao, Y. Zhang and J. Zhao, *ACS Catal.*, 2018, **8**, 1186–1191.
15 S. Mukherjee, D. A. Cullen, S. Karakalos, K. Liu, H. Zhang, S. Zhao, H. Xu, K. L. More, G. Wang and G. Wu, *Nano Energy*, 2018, **48**, 217–226.
16 M. Zhang, C. Choi, R. Huo, G. Gu, S. Hong, C. Yan, S. Xu, A. W. Robertson, J. Qiu, Y. Jung and Z. Sun, *Nano Energy*, 2020, **68**, 104323.
17 L. Zhang, L. X. Ding, G. F. Chen, X. Yang and H. Wang, *Angew. Chem.*, 2019, **131**, 2638–2642.
18 Q. Fan, C. Choi, C. Yan, Y. Liu, J. Qiu, S. Hong, Y. Jung and Z. Sun, *Chem. Commun.*, 2019, **55**, 4246–4249.
19 M. Jia, S. Hong, T. Wu, X. Li, Y. Soo and Z. Sun, *Chem. Commun.*, 2019, **55**, 12024–12027.
20 M. Jia, Q. Fan, S. Liu, J. Qiu and Z. Sun, *Curr. Opin. Green Sustainable Chem.*, 2019, **16**, 1–6.
21 Y. Gao, Z. Han, S. Hong, T. Wu, X. Li, J. Qiu and Z. Sun, *ACS Appl. Energy Mater.*, 2019, **2**, 6071–6077.
22 Z. Zhao, S. Hong, C. Yan, C. Choi, Y. Jung, Y. Liu, S. Liu, X. Li, J. Qiu and Z. Sun, *Chem. Commun.*, 2019, **55**, 7171–7174.
23 H. Tao, C. Yan, A. Robertson, Y. Gao, J. Ding, Y. Zhang, T. Ma and Z. Sun, *Chem. Commun.*, 2017, **53**, 873–876.
24 Y. Wu, Q. Zhang, X. Yin and H. Cheng, *RSC Adv.*, 2013, **3**, 9670–9676.
25 Y. Wang, K. Jia, Q. Pan, Y. Xu, Q. Liu, G. Cui, X. Guo and X. Sun, *ACS Sustainable Chem. Eng.*, 2018, **7**, 117–122.
26 R. Zhang, X. Ren, X. Shi, F. Xie, B. Zhang, X. Guo and X. Sun, *ACS Appl. Mater. Interfaces*, 2018, **10**, 28251–28255.

27 K. Jia, Y. Wang, Q. Pan, B. Zhong, Y. Luo, G. Cui, X. Guo and X. Sun, *Nanoscale Adv.*, 2019, **1**, 961–964.
28 J. Zhang, L. Yang, H. Wang, G. Zhu, H. Wen, H. Feng, X. Sun, X. Guang, J. Wen and Y. Yao, *Inorg. Chem.*, 2019, **58**, 5414–5418.
29 G. Yu, H. Guo, W. Kong, T. Wang, Y. Luo, X. Shi, A. Asiri, T. Li and X. Sun, *J. Mater. Chem. A*, 2019, **7**, 19657.
30 J. Zhao, L. Zhang., X. Xie, X. Li, Y. Ma, Q. Liu, W. Fang, X. Shi, G. Cui and X. Sun, *J. Mater. Chem. A*, 2018, **6**, 24031–24035.
31 Y. Luo, G. Chen, L. Ding, X. Chen, L. Ding and H. Wang, *Joule*, 2019, **3**, 279–289.
32 L. Yang, T. Wu, R. Zhang, H. Zhou, L. Xia, X. Shi, H. Zheng, Y. Zhang and X. Sun, *Nanoscale*, 2019, **11**, 1555–1562.
33 W. Shan, F. Liu, H. He, X. Shi and C. Zhang, *ChemCatChem*, 2011, **3**, 1286–1289.
34 E. Skulason, T. Bligaard, S. Gudmundsdóttir, F. Studt, J. Rossmeisl, F. Abild-Pedersen, T. Vegge, H. Jonsson and J. K. Nørskov, *Phys. Chem. Chem. Phys.*, 2012, **14**, 1235–1245.
35 J. H. Montoya, C. Tsai, A. Vojvodic and J. K. Nørskov, *ChemSusChem*, 2015, **8**, 2180–2186.
36 C. Choi, S. Back, N.-Y. Kim, J. Lim, Y.-H. Kim and Y. Jung, *ACS Catal.*, 2018, **8**, 7517–7525.